

Article

The Frequency Control Strategy of a Wind–Storage Combined System Considering Battery SOC

Xi Wang ^{1,*}, Xi Ye ², Wei Wei ¹, Yanfeng Wang ², Tong Zhu ², Chang Liu ³  and Yufan Chen ³¹ State Grid Sichuan Electric Power Research Institute, Chengdu 610000, China² State Grid Sichuan Electric Power Company, Chengdu 610000, China³ Sichuan New Electric Power System Research Institute, Chengdu 610000, China

* Correspondence: wangxi_sgcc@163.com

Abstract: The wind power capacity has increased a lot recently and the number of close energy storage systems has also rapidly increased. To enhance the frequency stability support ability of such wind–storage combined systems, this paper proposes a virtual synchronous control strategy for a wind–storage combined system considering the battery state of charge (SOC). The virtual synchronous control is used to make the wind turbine generate more active power when the system is in disturbance. Most importantly, to ensure that the stored energy is used efficiently, the wide-area SOC concept of the energy storage system is considered, which is realized by designing the batteries with additional control that is related to the other batteries' SOCs. This means that the low-SOC energy storage system's power shortage can be compensated for by the high-SOC batteries. The above unified control enhances the wind–storage combined system's frequency supporting ability. According to the simulations, the frequency drop can be suppressed through the help of the virtual synchronous control and the stored energy. Additionally, the instability can also be eliminated when wide-area SOC is considered, such that the proposed efficiency and correctness are finally verified through the simulations.

Keywords: frequency control; wind–storage combined system; SOC; virtual synchronous control

Citation: Wang, X.; Ye, X.; Wei, W.; Wang, Y.; Zhu, T.; Liu, C.; Chen, Y. The Frequency Control Strategy of a Wind–Storage Combined System Considering Battery SOC. *Electronics* **2023**, *12*, 3453. <https://doi.org/10.3390/electronics12163453>

Academic Editor: Carlos Andrés García-Vázquez

Received: 3 July 2023

Revised: 6 August 2023

Accepted: 7 August 2023

Published: 15 August 2023



Copyright: © 2023 by the authors. Licensee MDPI, Basel, Switzerland. This article is an open access article distributed under the terms and conditions of the Creative Commons Attribution (CC BY) license (<https://creativecommons.org/licenses/by/4.0/>).

1. Introduction

The total installed capacity of renewable energy in China had reached 190.87 million kilowatts by the end of 2020, an increase of 85.87 million kilowatts compared with the previous year and a year-on-year growth rate of 81.8%. The newly added capacity of grid-connected wind and solar power generation units was 119.87 million kilowatts, exceeding the total scale of newly added units in the previous year. However, the newly added capacity of thermal power units, including coal-fired power and biomass power generation, accounted for 29.53% of the total newly added capacity, a decrease of 21 percentage points compared with 2015 [1–3]. By the end of the 14th Five-Year Plan, it is expected that the installed capacity of renewable energy generators will account for more than 50% of the total installed capacity of China's electricity [4]. At that time, the role of renewable energy in China's development will shift from being a supplementary alternative energy source (as it has been in the past) to being the main energy source for market consumption. According to the statistics of the Global Wind Energy Council, China's wind power penetration is expected to reach about 15% in 2035.

Due to the volatility and randomness of wind power itself, large-scale wind power integration will reduce the grid inertia and make the stability become worse [5]; therefore, the phenomenon of wind abandonment is serious. Considering the rapid development of power electronics and batteries in China and the wide application of battery energy storage, it has become an important development direction in the field of new energy to build large-capacity energy storage systems for wind farms to achieve free and flexible

control of wind farms and establish a wind storage system with strong controllability and a flexible operation mode.

At present, the research on doubly fed wind turbines at home and abroad mainly focuses on reactive power regulation technology, active frequency modulation technology and wind power prediction technology. On the reactive power regulation area, the literature [6] proposed presents a dynamic coordination control strategy to enhance the reactive power capability of wind power plants (WPPs) that deploy doubly fed induction generator-based wind turbines (DFIG-WTs). The proposed control architecture seeks to maximize the reactive power availability during grid faults without violating the stable and thermal operational limits of the generator. Reference [7] describes a mixed integer dynamic optimization-based method for optimal dynamic reactive power allocation in large-scale wind integrated power systems. One of the important aspects of the proposed methodology is that unlike static optimal power flow-based approaches, the proposed method considers detailed system dynamics and the wind turbine grid code compliance while optimizing the allocation of dynamic reactive power sources. To satisfy the reactive power demand of the system under wind speed variations, coordinating the reactive power capability and active power output of wind farm is the key solution. Based on this, a novel active control idea is proposed by [8]. The reactive power capability of wind farms and the reactive power demand of the system are both studied; additionally, the controllable conditions of access point voltage are analyzed. Active voltage control strategies, including active adjustment of reactive power reference, active speed control and active pitch angle intervention according to wind speed ranges, are proposed.

In terms of the active frequency modulation area, reference [9] proposes the introduction of droop control in the rotor side control mode of the doubly fed wind turbine, so that the wind turbine can support the voltage and frequency in the process of a black start. It is verified by experiments that the new control technology can effectively stabilize the voltage and frequency of the grid-connected point when the wind turbine is off the grid. By analyzing the internal power change of the doubly fed wind turbine during grid-connected operation, a method of using the computer to simulate the upper and lower limits of reactive power is proposed. The study in [10] describes the modeling of power smoothing and frequency controlling in wind plants and assesses different control strategies as well as the grid frequency performance gains achievable over hydropower islanding systems and over islanding systems incorporating both hydropower and conventional wind plants. The results showed that wind plant power output could be smoothed in a short time frame and that the support frequency in both the primary and secondary frequency control timescales included droop functionality. The authors of [11] proposed an active power hierarchical control method based on different unit capacity ratios. Additionally, a frequency regulation strategy for wind power based on limited overspeed de-loading curve partitioning was proposed. On the basis of the rotor kinetic energy control, the relationship between the de-loading capacity of the overspeed control and wind speed was studied. Combined with the data fitting, the limited overspeed de-loading level curve of the WT was obtained to partition overspeed de-loading and pitch de-loading; this approach maximizes the use of overspeed de-loading and enhances the frequency regulation capacity of the WT [12]. In addition, some studies have also applied frequency control to practical engineering; the experimental results of a secondary frequency regulation test carried out on a 10 MW wind farm with type-V wind turbines is shown in [13]. This was a 5 h test of the wind farm's ability to follow an external, historical, automatic generation control signal. A total of 1 MW of power was offered on the regulation market with upregulation provided via a fixed curtailment value. The performance of the farm was evaluated using the performance score method developed by the Pennsylvania–New Jersey–Maryland (PJM) system operator. The performance scores were used to perform an economic analysis using 2017 hourly PJM price data.

For wind power prediction technology, different time-scale predictions are studied, such as the short-term wind power prediction based on the particle swarm optimization–

extreme learning machine model combined with the AdaBoost algorithm [14], the ultra-short-term wind power prediction considering source relevance [15] and so on.

For wind–storage combined systems, the focus at home and abroad is on the use of energy storage systems to suppress the power fluctuations of wind farms and energy storage systems participating in system frequency adjustment and capacity optimization. In reference [16], the most recent advances in LFC techniques for wind-based power systems are examined. Moreover, the use of classical, artificial intelligence, model predictive control, a sliding mode control, cascade controllers and other newly designed and adopted controllers in the LFC area is thoroughly examined. In [17], a capacity configuration scheme for an energy storage system based on the cross ion swarm optimization algorithm is proposed, and the wavelet packet decomposition method is used to collect the operating parameters of the wind farm and establish the optimal mathematical model. Some researchers have also proposed a capacity configuration method for the energy storage system to stabilize the active output of the wind farm. This method established a two-way optimization model of frequency and capacity and found the optimal capacity configuration parameters to meet the requirements of stabilization by low-pass filtering [18]. Reference [19] proposes real-time optimized dispatch strategies for automatic generation control (AGC) to utilize wind power and the storage capacity of electric vehicles for the active power balancing services of the grid. The proposed dispatch strategies enable the AGC to appropriately allocate the regulating reserves from wind power plants and electric vehicles, considering their operational constraints. In [20], a power control method based on model prediction technology is proposed. The output power of a wind farm can be dispatched according to the real-time demand of power grid. By combining FACTS devices with an energy storage system, the influence of wind farm fluctuation is reduced and the power quality improved. In addition, some research related to the aging mechanism of batteries has also been conducted, such as the accelerated aging mechanisms of the Li (NiCoMn) O₂ (NCM) battery, which were analyzed by the nondestructive quantitative diagnostic method [21]. Additionally, ref. [22] proposes an integrated battery life loss modeling and anti-aging energy management (IBLEM) method for improving the total economy of BESS in EVs. In the above literature, the wind farm is used as the constant power source of the system. The main function of the energy storage system is to suppress the fluctuation of the wind farm and then optimize the output power under the fluctuation of the wind turbine.

It can be found that the above studies usually consider wind power and battery storage in the traditional style. In particular, these studies pay much more attention to wind power and the battery storage's characteristic is usually ignored. However, it is known that the battery has its own state-of-charge (SOC) index, which is one key index for its output ability assessment. Even if some studies have considered the SOC of a single energy storage system, the unified control structure is not established. To solve such problem, this paper proposes the frequency control strategy of a wind–storage combined system considering the different battery storage system's SOC, such that the wind–storage combined system can use the frequency support ability of the wind power and high-SOC batteries efficiently. Specifically, virtual synchronous control is used to make the wind turbine generate more active power when system is in disturbance and the wide-area SOC concept of the energy storage system is considered to make the batteries be used more reasonably. According to the simulations, the frequency drop can be suppressed through the help of the virtual synchronous control and the stored energy. Additionally, the instability can also be eliminated when wide-area SOC is considered.

The structure of the paper is as follows. Section 2 introduces the basic structure of energy storage and wind power system. Section 3 then proposes the coordinated control scheme considering battery SOC. In Section 4, the simulations are implemented to prove the proposed schemes, and Section 5 concludes the paper.

2. The Basic Structure of the Energy Storage and Wind Power System

2.1. The Structure of the Energy Storage System

The model of the energy storage system is divided into two parts: the battery system and the power conversion system. The battery system model is mainly divided into a chemical model and a circuit model, whereas the power conversion system is divided into a DC/AC direct connection type and a DC/AC-DC/DC mixed connection type based on different types of intermediate inverters.

At present, mainstream battery energy storage systems usually use lithium iron phosphate batteries with higher energy density and better safety; this type of battery is not easy to decompose. The battery energy storage system achieves power exchange with the external power grid by absorbing and storing energy. Due to the low voltage and limited energy density of a single battery, multiple battery cells are usually connected in series to form a battery system [14]. The power conversion system serves as a carrier for the power exchange, connecting the battery system and the external power grid and achieving bidirectional energy transfer.

The research focus of this article is on the electrical process of the battery system participating in a black start. Therefore, the equivalent circuit models are used for modeling. Currently, the main types of models include the Thevenin equivalent model and the fourth-order dynamic model [15]. The Thevenin model is mainly used for dynamic analysis of simple battery systems. The fourth-order model has a deeper physical meaning and is more complex, making it suitable for practical simulation analysis of larger battery systems. Based on the actual requirements of this article, we establish a simpler and more easily obtainable model and fit the actual equivalent circuit model based on the constant current discharge characteristic curve of the battery pack. The constant current discharge characteristic curve of the battery pack is shown in Figure 1.

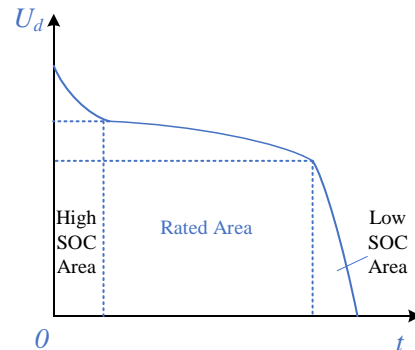


Figure 1. Constant current discharge characteristic curve of a battery.

According to the above figure, the initial voltage rapidly decreases in the high-SOC area and enters the rated operating zone in a short period of time. A longer rated characteristic zone can ensure that the battery maintains a longer lifespan during use. As the discharge period approaches, the terminal voltage of the battery rapidly decreases in a short period of time. By fitting the constant current discharge characteristic curve of the battery, an equivalent circuit model can be obtained, as shown in Figure 2.

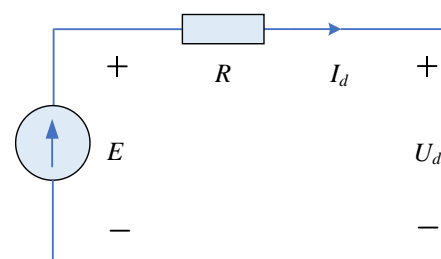


Figure 2. Battery system equivalent circuit model.

From the above figure, it can be seen that the circuit model of the battery can be represented as a series structure of voltage source E and equivalent internal resistance R . The equivalent internal resistance R is determined by the manufacturer at the time of production and remains unchanged during operation. The controlled voltage source E can be represented as:

$$E = E_0 - \frac{KC_{\max}}{C_{\max} - Q_c} + A \exp(-B \otimes Q_c) \quad (1)$$

In the formula, E_0 represents the potential within the battery system, A , K and B respectively represent fitting parameters, $A \exp(-B \otimes Q_c)$ represents the initial discharge characteristics of the battery, Q_c represents the discharge capacity and C_{\max} represents the maximum battery capacity.

At present, the main power conversion system models include DC/AC–DC/DC hybrid connections or DC/AC direct connections. This paper uses the DC/AC direct connection type for study.

The structure diagram of the DC/AC direct connection type is shown in Figure 3. This structure connects the battery system to the PWM converter and directly connects to the power grid through a step-up transformer, which plays a role in matching the voltage and isolation. This type of power conversion system has a simple structure and is suitable for various distributed independent system grid connection processes as it has lower energy consumption during charging and discharging processes.

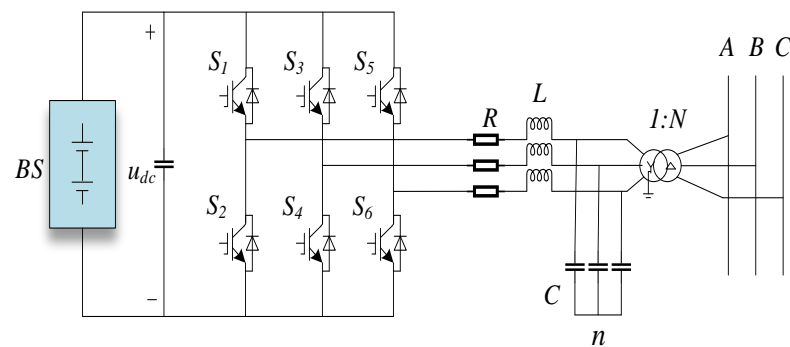


Figure 3. The basic structure of the energy storage system.

2.2. The Structure of Wind Power System

Wind power generation is achieved by converting wind energy into mechanical energy to drive the motor to rotate and output alternating current. Doubly fed induction generators (DFIGs) are currently the most widely used wind turbines in the world, with electrical structures including stator and rotor windings, as well as back-to-back PWM converters on the rotor windings. Its mechanical structure includes wind turbines, generators, directional controllers and other internal functional modules, such as a yaw system, electronic controller, hydraulic system and pitch system [16].

The DFIG mainly consists of wind turbine blades, a gearbox, a doubly fed generator, a back-to-back PWM converter, etc., as shown in Figure 4. The doubly fed fan maintains voltage stability at the fan outlet through the control system on the stator and rotor sides. When the parameters at the fan outlet match the system parameters, the switch k is closed and the fan is smoothly integrated into the system.

As for the type of the turbine for wind power, this paper uses horizontal axis wind turbines with variable pitch ability. The use of variable pitch technology in wind turbines can greatly improve the stress conditions of the blades and the entire machine, which is very beneficial for large wind turbines.

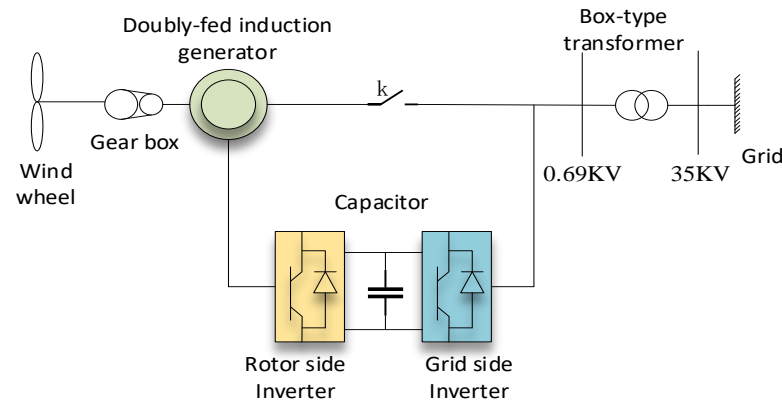


Figure 4. The basic structure of the DFIG.

The three-phase stator winding voltage equations, three-phase rotor winding voltage equations and the flux linkage equations of the DFIG are as follows.

$$\begin{cases} u_{sA} = R_s i_{sA} + \frac{d\psi_{sA}}{dt} \\ u_{sB} = R_s i_{sB} + \frac{d\psi_{sB}}{dt} \\ u_{sC} = R_s i_{sC} + \frac{d\psi_{sC}}{dt} \end{cases} \quad (2)$$

$$\begin{cases} u_{rA} = R_r i_{rA} + \frac{d\psi_{rA}}{dt} \\ u_{rB} = R_r i_{rB} + \frac{d\psi_{rB}}{dt} \\ u_{rC} = R_r i_{rC} + \frac{d\psi_{rC}}{dt} \end{cases} \quad (3)$$

$$\begin{cases} \psi_s = L_s I_s + L_m I_r \\ \psi_r = L_m I_s + L_r I_r \end{cases} \quad (4)$$

In the above equations, U_s and U_r represent the stator and rotor voltages, respectively; R_s and R_r represent the stator and rotor resistance, respectively; I_s and I_r represent the stator and rotor currents, respectively; Ψ_s and Ψ_r represent the stator and rotor flux linkages, respectively; L_s , L_r and L_m represent the self-inductance of stator and rotor and the mutual inductance between stator and rotor, respectively; and ω_N and ω_{slip} represent the rated speed and speed difference, respectively.

3. The Coordinated Control Scheme Considering the Battery SOC

3.1. The Basic Control Scheme of the Energy Storage System

The control mode of the battery energy storage system is divided into grid-connected mode and island mode according to the state of the external power grid. When the power grid works in a normal state and has its own voltage and frequency support, the energy storage system adopts grid-connected control.

When the energy storage system operates in grid-connected mode, the grid provides voltage and frequency support, which is essentially P/Q control. The energy storage system outputs the corresponding power according to the given active and reactive power reference values. The control block diagram is shown in Figure 5.

P_{Bref} is the active power reference to send out, P_B is the measured outputting active power, Q_{Bref} is the reactive power reference to send out, Q_B is the measured outputting reactive power, i_{Bdref} is the active outer loop current reference, i_{Bd} is the measured outer loop active current, i_{Bqref} is the reactive outer loop current reference and i_{Bq} is the measured reactive outer loop current.

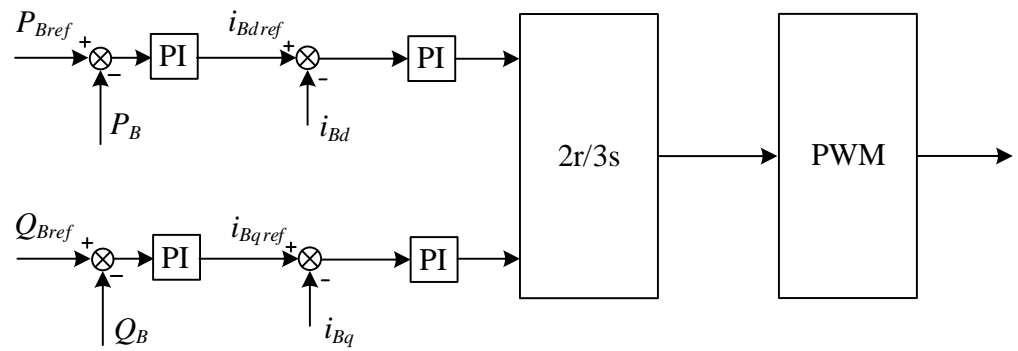


Figure 5. The basic control diagram of the energy storage system.

3.2. Wind Power with Virtual Synchronous Control

This article applies virtual synchronous control to the rotor side converter of wind turbines. The advantage of virtual synchronous control over conventional control is that by simulating the rotor motion equation of a synchronous generator, the rotor can store or release kinetic energy in the event of fluctuations in the system’s active power, such as large-scale input or removal of loads, reducing the imbalance of active power, providing better support for frequency and improving system stability.

The rotation equation of virtual synchronous control is achieved by imitating the motion equation of the generator rotor:

$$P_e^{ref} - P_e^m = T_j \frac{d\omega}{dt} \tag{5}$$

where P_e^{ref} and P_e^m represent the reference value and measured value of electromagnetic power, respectively, T_j represents the moment of inertia and ω indicates the speed. From this formula, it can be seen that an inverter with virtual synchronous control can reduce the imbalance of active power by changing the rotor speed when switching loads, generators, etc., thus playing a good role in supporting the frequency.

The virtual synchronization control adopted in this paper is shown in Figure 6; this includes frequency control and voltage control. Its mechanism can be found in the following equations:

$$(\omega_N - \omega_1) \frac{1}{m} + P_{ref} - P_m - P_D = J_\Delta \frac{d\omega_0}{dt} \tag{6}$$

$$P_D = D_1(\omega_0 - \omega_1) \tag{7}$$

$$\theta_r = \int \omega_{slip} dt \tag{8}$$

$$\omega_{slip} = \omega_0 - \omega_r \tag{9}$$

where ω_N is the rated frequency; ω_1 represents the actual angular frequency; ω_0 represents the internal potential angle frequency; M is the droop coefficient, which represents the droop effect of the frequency regulator f/P ; P_{ref} refers to the reference value of the active power; P_m refers to the measured value of the active power; P_D represents the damping power; D_1 represents the damping coefficient; J_Δ represents the virtual inertia constant and ω_{slip} represents the slip angle frequency.

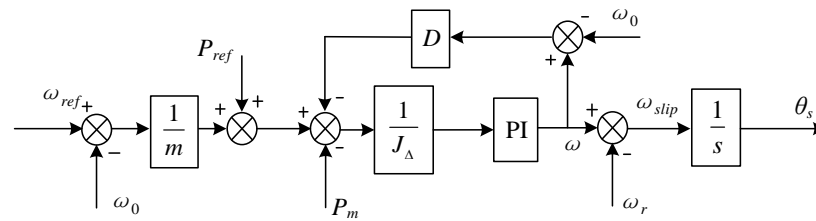


Figure 6. The virtual synchronous control diagram.

In this paper, the single mass model is used for the fan. Equation (6) represents the virtual rotation equation of the fan, which simulates the inertia characteristics, droop characteristics and damping characteristics of the synchronous generator. Through the virtual rotation equation, the fan shows inertia similar to that of the synchronous generator. From the virtual rotation equation, it can be seen that when the rated power output by the fan is different from the power required by the load, the DFIG can increase or decrease the released kinetic energy by adjusting its own speed, thus inhibiting the oscillation of active power and improving the support effect on frequency. Equation (7) represents the damping equation of the DFIG, which simulates the damping characteristics of a synchronous generator.

From the virtual rotation equation, it can be seen that when the rated power output of the fan is different from the power required by the load, such as during the switching of a large capacity unit, the cutting off of a large capacity load or a system malfunction, the DFIG increases or decreases the released kinetic energy by adjusting its own speed, changes the virtual internal potential angle frequency and adjusts the rotor speed to suppress the active power oscillation and improve its support for frequency. The specific control block diagram is shown in Figure 6.

3.3. The Co-Ornidated Control Scheme Considering the SOC

3.3.1. The Supplementary Frequency Control of the Energy Storage System

As mentioned above, the storage system can control its output active and reactive power. Therefore, to enhance its support ability for the AC system, supplementary control can be added. Specifically, the supplementary frequency control can be designed and added to its active power control loop.

The supplementary control of the energy storage system is presented in Figure 7. It can be seen that besides the regular active power control loop, the P_{added} control loop is added. This control loop generates the additional active power to the base reference value to eliminate the frequency deviations. The input of the supplementary control is the difference in the frequency; the f is the measured system frequency, and 50 Hz is the base value. The frequency is firstly sent to a low-frequency filter to decrease the noise, where the G is the filter gain and the T is the time constant. Then the dead zone is applied to make sure the control can only be triggered once the frequency difference is large enough; a 0.02 Hz dead zone is designed, which means the frequency value can only be active when the frequency deviation reaches 0.02 Hz. After that, the frequency deviation is transmitted to a PI controller and the final active power order to be added is generated.

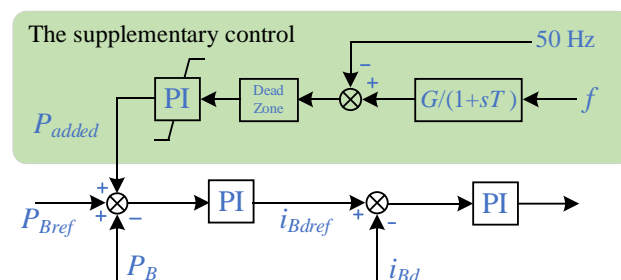


Figure 7. The supplementary control of the energy storage system.

3.3.2. The Coordinated Control Strategy of Battery Energy Storage Considering SOC

At present, most studies focus on using battery energy storage to simulate conventional generator units to improve the effect of frequency regulation, that is, battery energy storage can work like conventional generators. However, battery energy storage has its own characteristics, such as the SOC (state of charge). The SOC of a battery refers to the state of the remaining battery charge. Generally, the SOC of a battery should remain in a reasonable zone to ensure its normal operation. However, the energy storage system usually only considers its own SOC rather than considering it in a wide area. This is a disadvantage that may lead to a lack of active power support when a battery reaches a relatively low SOC and no active power can be generated.

To overcome such a shortage, this paper proposes a wide-area multi-SOC concept to guarantee the battery’s output when different energy storage systems are applied to the electric grid. The detailed control strategy can be presented, as Equations (10) and (11) shows.

$$K_{add}(SOC) = \begin{cases} P_{added}, & SOC < 10\% \\ 0, & SOC \geq 10\% \end{cases} \quad (10)$$

$$K_{self}(SOC) = \begin{cases} P_{extra}, & SOC \geq 50\% \\ 0, & SOC < 50\% \end{cases} \quad (11)$$

It can be seen from Equation (10) that, besides the basic supplementary frequency control, the wide-area SOC from the other battery storage system are considered. This control can make sure that once some batteries are out of work, the other energy storage systems can increase their output to avoid power shortages. Thus, the frequency stability can be guaranteed. On the other hand, Equation (11) makes sure that such a wide-area supplementary control is active only when the battery’s SOC is big enough, i.e., above 50%.

In Figure 8 and Equations (10) and (11), the K_{add} function is the wide-area SOC considered control, the K_{self} function is the self SOC considered control, P_{extra} is the output of the wide-area control and P_{addi} ($i = 1, 2, 3, \dots$) is the final output of the supplementary frequency control.

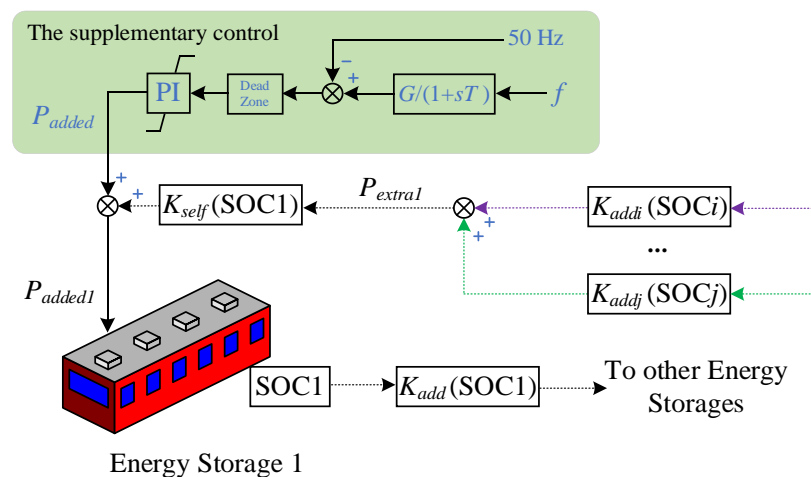


Figure 8. The supplementary frequency control scheme based on wide-area SOC.

3.3.3. The Unified Coordinated Control Strategy Considering the SOC and Virtual Synchronous Control

To further enhance the frequency stability of the power system, the unified coordination control strategy between the wind power and energy storage system is also proposed.

It can be seen from Figure 9 that the whole control strategy consists of two parts. The first part is the virtual synchronous control of the wind power; this control can reduce the impact of the wind power fluctuations and enhance its frequency support to the power system when the disturbance happens, as the virtual inertia can make the wind power act

like a regular generator. The second part of the unified coordinated control strategy is the supplementary frequency control based on the battery energy storage system. This part of the scheme not only makes the battery actively support the power grid but can also make the battery energy storage consider the SOCs of the other storage systems. Such a design allows the renewable power and its storage system act together.

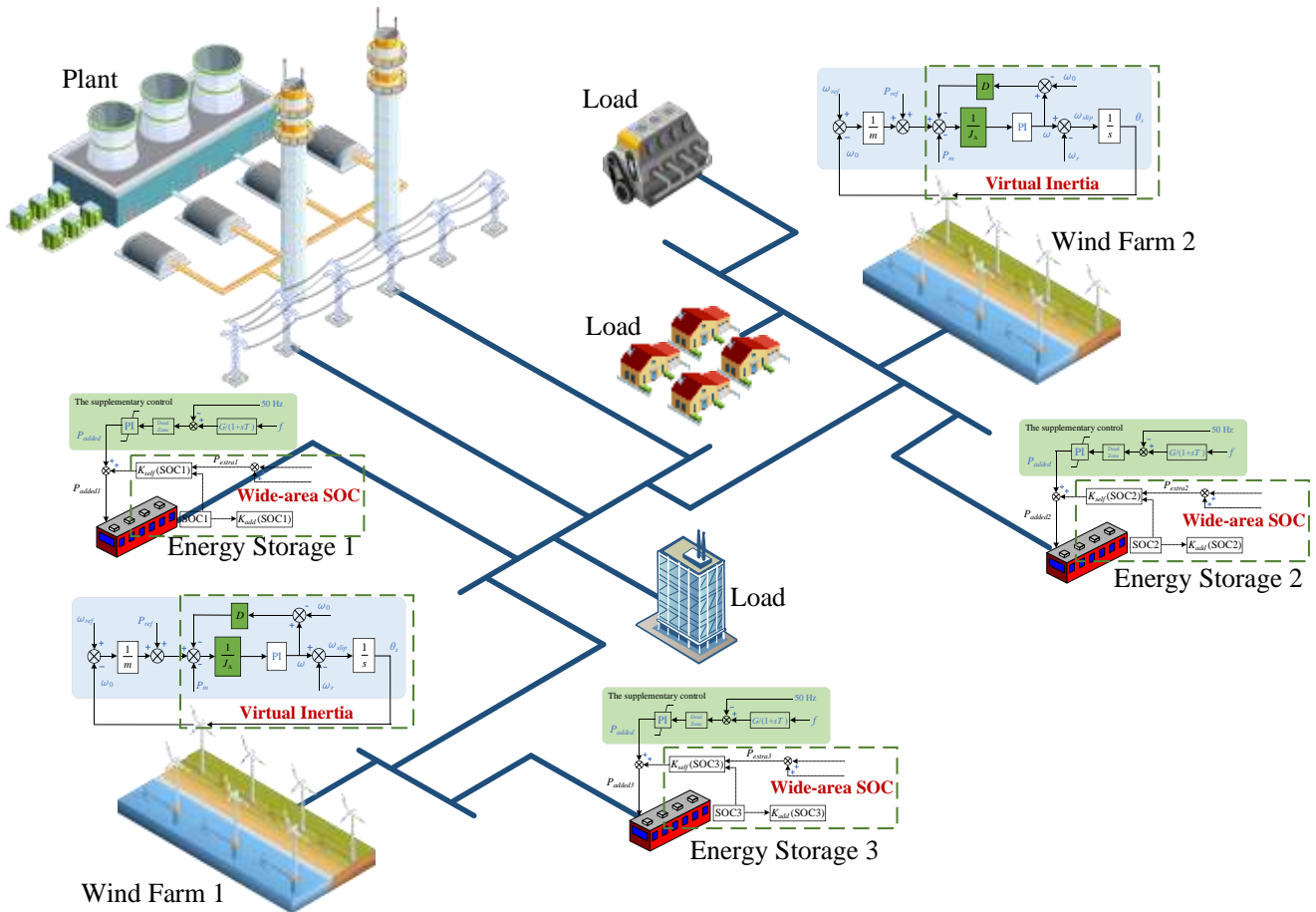


Figure 9. The unified coordinated control strategy.

4. Case Study

To verify the previously proposed coordination scheme, case studies are implemented in this section. The topology of the test model is presented in Figure 9. It can be seen that there are three battery energy storage systems, two wind farms, one equivalent generator and some loads. The parameters of the system can be found in Table 1.

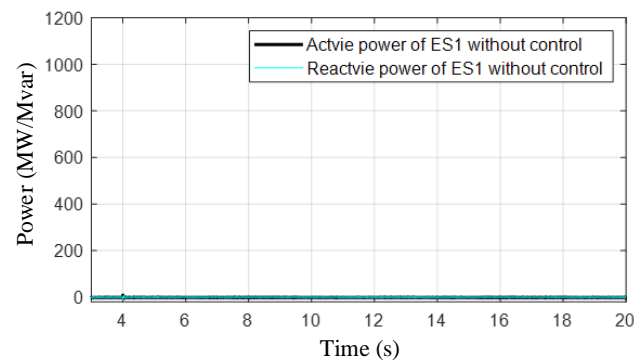
The simulations are implemented in three different conditions. In the first condition, a 2100 MW load is put in at 4 s and no supplementary control is added. In the second condition, when the 2100 MW load is put in at 4 s, the virtual synchronous control of the wind farm and the traditional supplementary control of energy storage systems are added, which is named as the traditional control. In the third condition, when the 2100 MW load is put in at 4 s, the virtual synchronous control of the wind farm and the supplementary control considering wide-area SOCs of energy storage systems are added, which is named as the proposed control. All the loads mentioned above are fixed-type loads, and the load variation is achieved by increasing the load parameters when simulations are implemented. Figures 10–18 show the simulation results of different signals, which will be analyzed and compared in the next sections.

Table 1. The parameters of the test system.

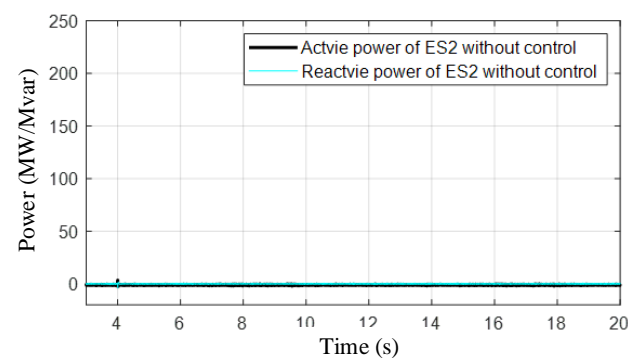
Equipment	Parameter	Value
Energy storage 1	Rated Capacity	1200 MW
	Rated DC voltage	200 kV
	Rated AC voltage	500 kV
	Initial SOC (equivalent)	90%
Energy storage 2	Rated Capacity	250 MW
	Rated DC voltage	200 kV
	Rated AC voltage	500 kV
	Initial SOC (equivalent)	22%
Energy storage 3	Rated Capacity	250 MW
	Rated DC voltage	200 kV
	Rated AC voltage	500 kV
	Initial SOC (equivalent)	31%
Wind farm 1 and 2	Rated Capacity	1200 MW
	Rated AC voltage	500 kV
Equivalent Generators	Rated Capacity	15,000 MW
	Rated AC voltage	500 kV

4.1. The Energy Storage System Simulation Results with No Additional Control

In Figure 10, the output active and reactive power of energy storage system 1 (ES1), energy storage system 2 (ES2) and energy storage system 3 (ES3) are presented. Figure 10 shows the results with no additional control, and it can be seen that the output of each energy storage remains zero. In addition, the equivalent SOC of each energy storage system does not change as no output is generated, which can be seen in Figure 11. The equivalent SOC here is used because the real SOC varies in hours, which cannot be simulated in electromagnetic transient software. The discharging characteristics of the batteries are modified to ensure that the SOC can change in seconds. This modification is acceptable and convenient for analysis.

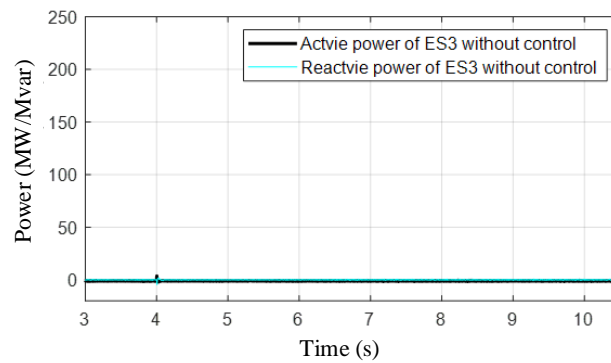


(a)



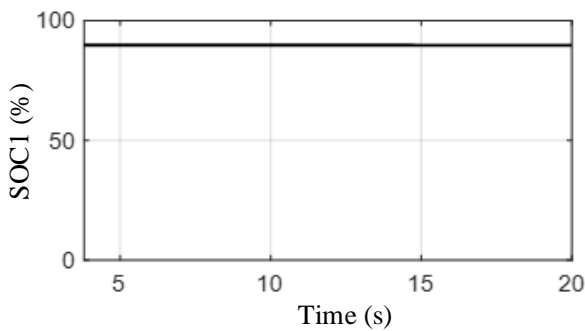
(b)

Figure 10. Cont.

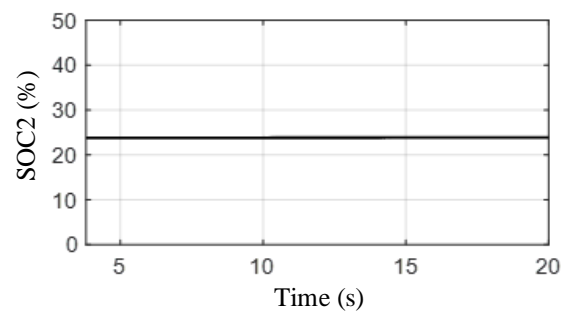


(c)

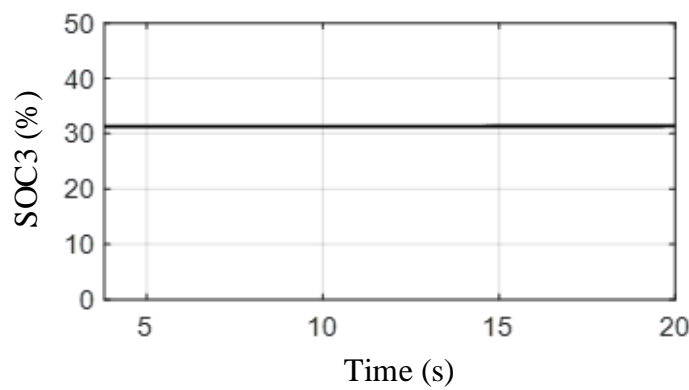
Figure 10. The output active and reactive power of different energy storage systems when no additional control is added. (a) The output of ES1 without control. (b) The output of ES2 without control. (c) The output of ES3 without control.



(a)



(b)



(c)

Figure 11. The equivalent SOC of different energy storage systems when no additional control is added. (a) The equivalent SOC of ES1 without control. (b) The equivalent SOC of ES2 without control. (c) The equivalent SOC of ES3 without control.

4.2. The Energy Storage System Simulation Results with Traditional Control

In Figure 12, the output active and reactive power of energy storage system 1 (ES1), energy storage system 2 (ES2) and energy storage system 3 (ES3) are presented when traditional supplementary control is added. It can be seen that the outputs begin to oscillate after a while. This is because the traditional control does not consider the SOC of the other battery storage systems. According to Figure 13, ES2 and ES3 decrease to a relative low value (12%), the output of the battery becomes less and the system has no other support, meaning that oscillation occurs.

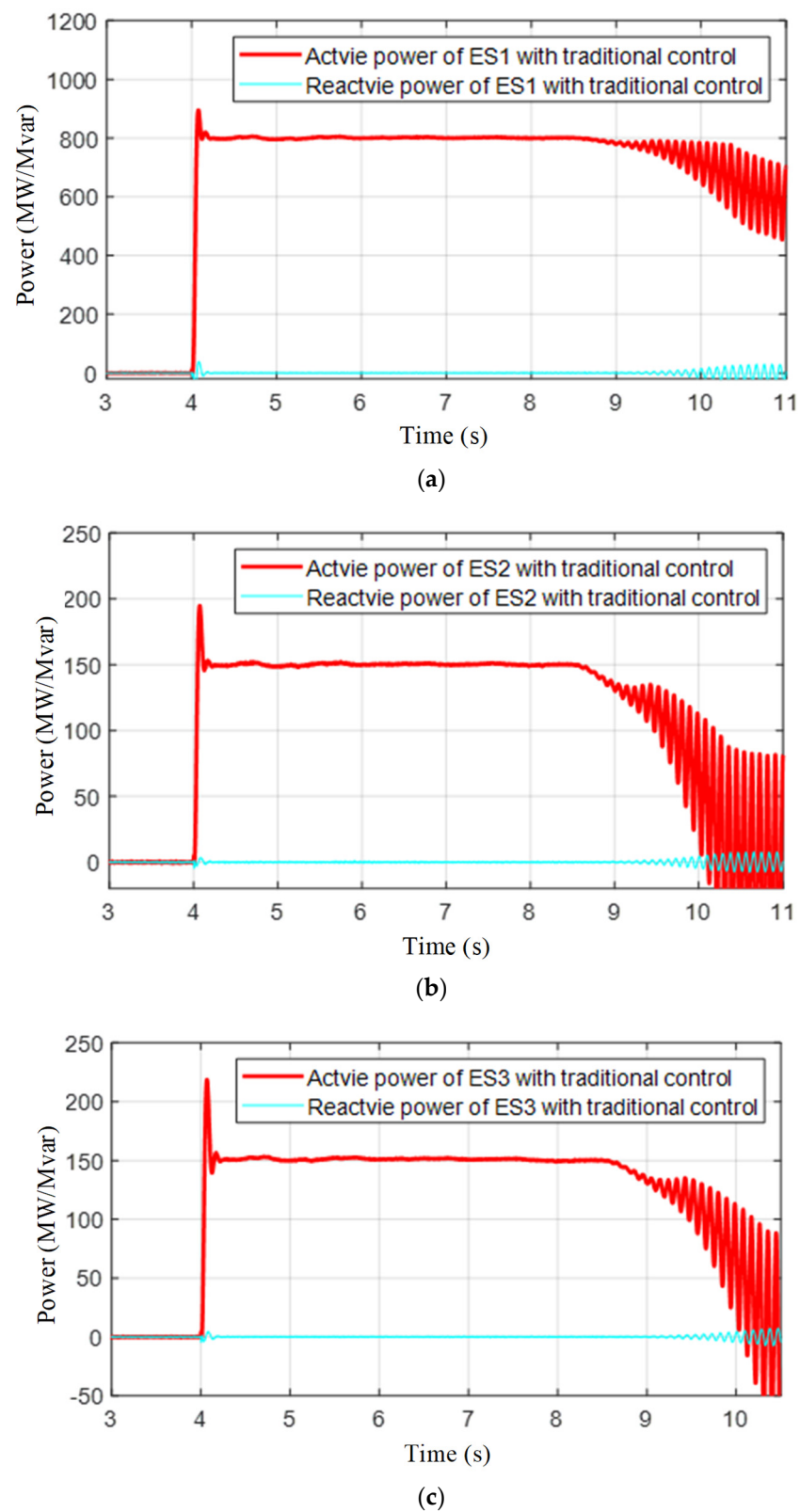


Figure 12. The output active and reactive power of different energy storage systems when only traditional control is added. (a) The output of ES1 with traditional control. (b) The output of ES2 with traditional control. (c) The output of ES3 with traditional control.

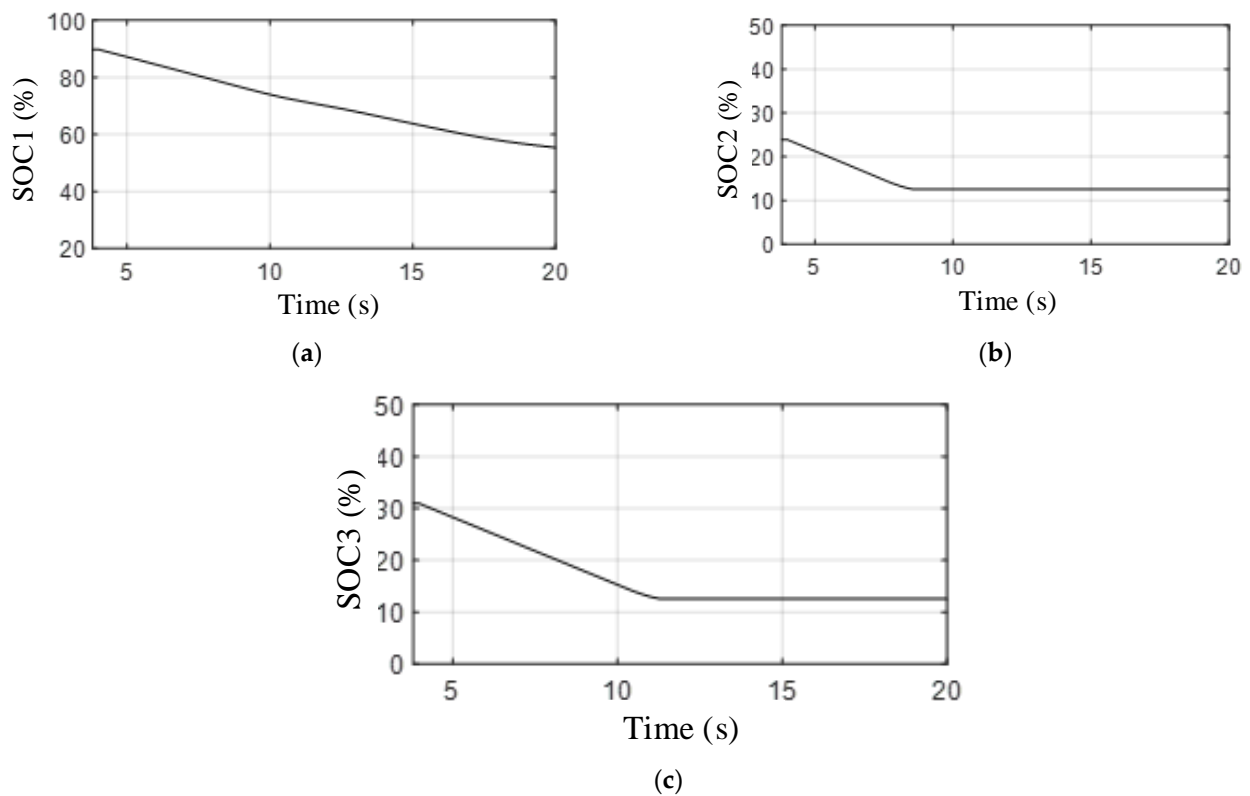


Figure 13. The equivalent SOC of different energy storage systems when only traditional control is added. (a) The equivalent SOC of ES1 with traditional control. (b) The equivalent SOC of ES2 with traditional control. (c) The equivalent SOC of ES3 with traditional control.

4.3. The Energy Storage System Simulation Results with the Proposed Control

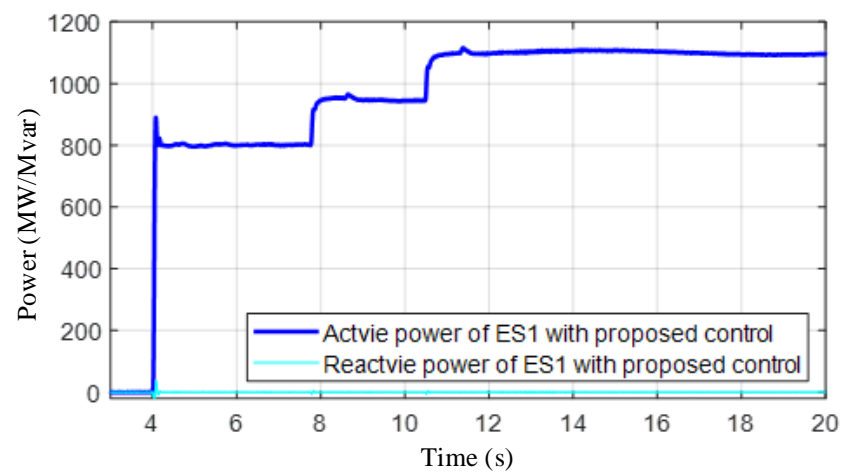
In Figure 14, the output active and reactive power of energy storage system 1 (ES1), energy storage system 2 (ES2) and energy storage system 3 (ES3) are presented when the proposed control is added. It can be seen that the outputs of ES1 increase accordingly when the other battery's SOC reaches low value. Additionally, the system can remain stable as the active power can be compensated. Figure 15 shows the SOC of each energy storage system.

Figure 16 presents the output of the wind power with and without virtual synchronous control. It can also be seen that the virtual synchronous control can make the wind power output a more active power so that the system can be more stable.

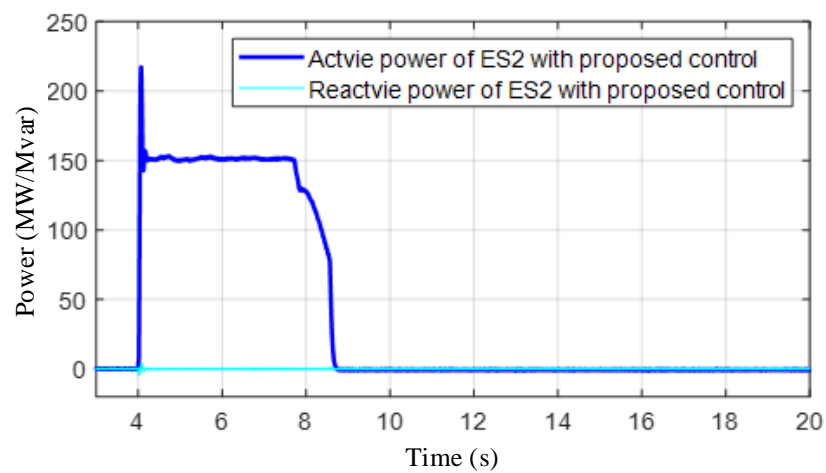
4.4. The AC Frequency Comparison in Different Control Conditions

From the above simulation results, it can be seen that the proposed method can generate more active power. This next section compares the AC side frequency with different control modes, which also proves the effectiveness and correctness of the proposed strategy.

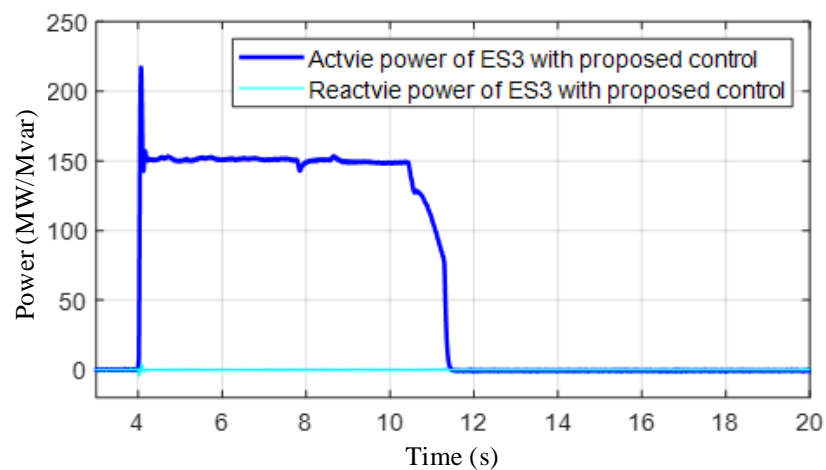
In Figure 17, it can be seen that in the transient 3.8 s and 4.6 s, the frequency disturbance can be decreased when additional controls are added, where about 0.01 Hz of fluctuation can be avoided. Moreover, the frequency can also recover faster. However, according to Figure 17, there is no difference between the proposed control and the traditional control in the transient period. Such a problem is addressed in Figure 18.



(a)



(b)



(c)

Figure 14. The output active and reactive power of different energy storage systems when the proposed control is added. (a) The output of ES1 with the proposed control. (b) The output of ES2 with the proposed control. (c) The output of ES3 with the proposed control.

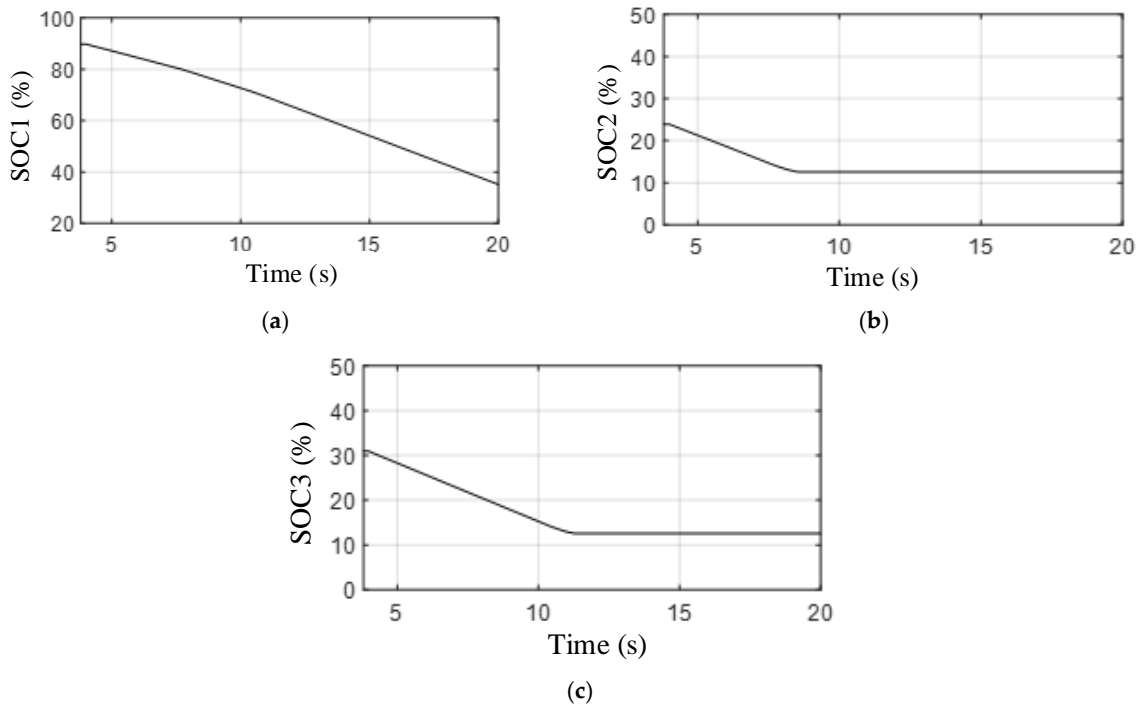


Figure 15. The equivalent SOCs of different energy storage systems with the proposed control. (a) The equivalent SOC of ES1 with the proposed control. (b) The equivalent SOC of ES2 with the proposed control. (c) The equivalent SOC of ES3 with the proposed control.

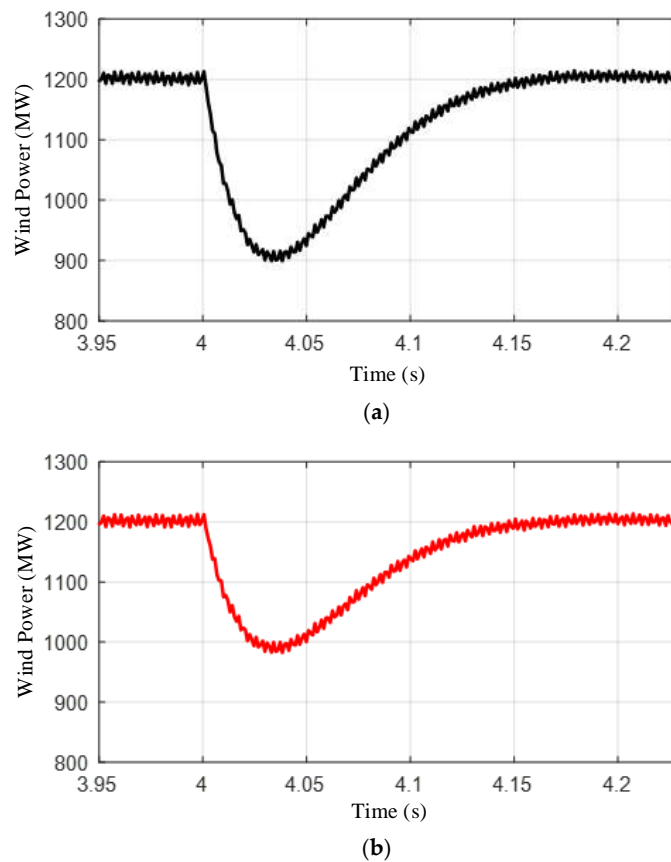
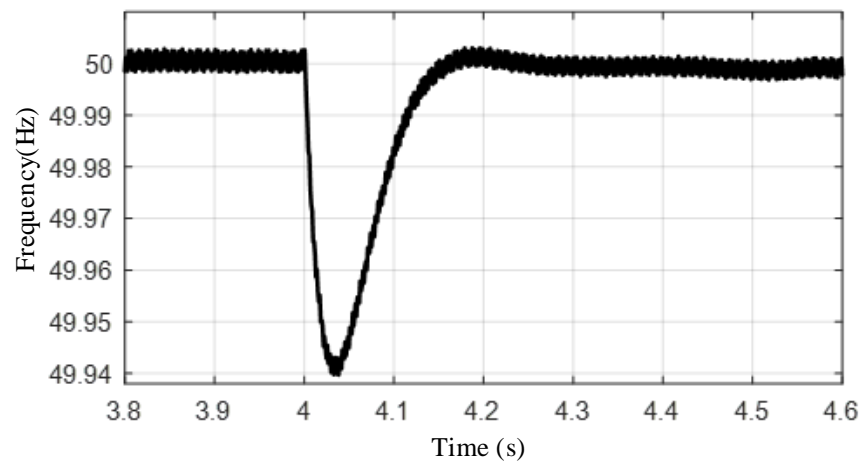
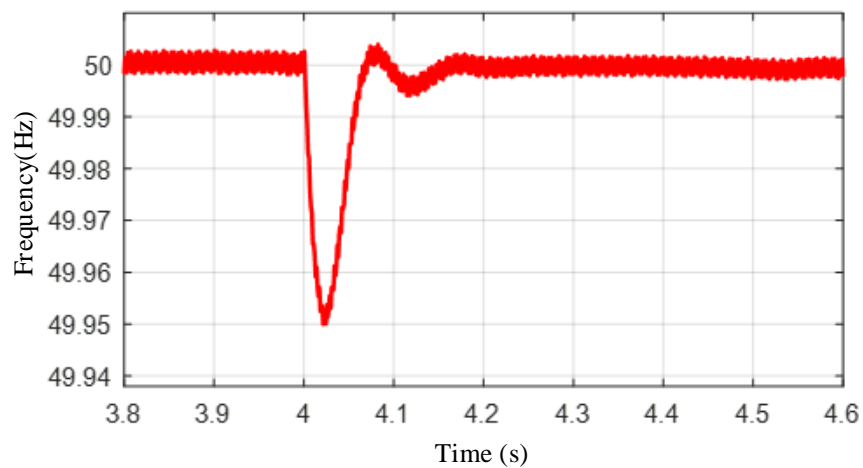


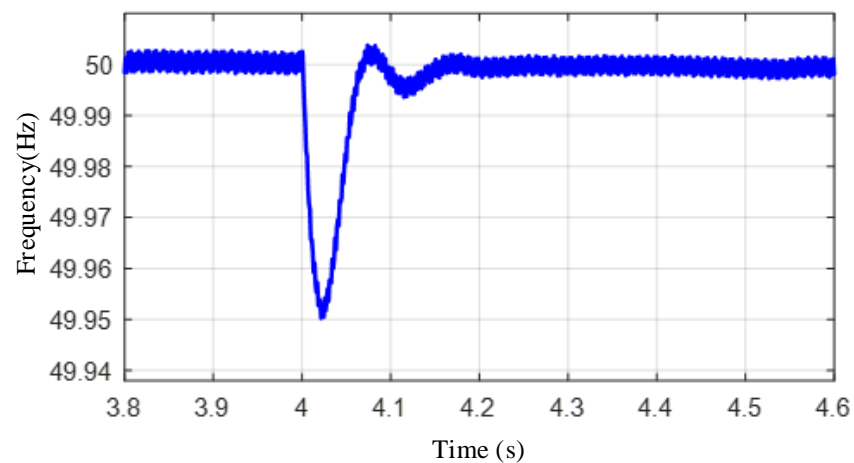
Figure 16. The output of the wind power with different controls. (a) The wind power without virtual synchronous control. (b) The wind power with virtual synchronous control.



(a)



(b)



(c)

Figure 17. The AC system frequency disturbance in case 1 simulation between 3.8 s and 4.6 s. (a) The frequency disturbance without control. (b) The frequency disturbance with traditional control. (c) The frequency disturbance with the proposed control.

In Figure 18, the frequencies in different conditions are shown in a relatively long period, namely 20 s. It can be observed that with traditional control the system finally

becomes unstable, whereas the proposed strategy can keep the frequency maintained at the rated value.

The oscillations occur because the AC system with converters is actually not so strong and the active power and the reactive power impact each other extensively. Once the disturbance occurs, the traditional control cannot generate more active power, making the AC side and the DC side both suffer from the power imbalance, which finally makes the storage oscillate and then causes the AC system to also become unstable. Compared with the no additional control and traditional control methods, the proposed strategy cannot only enhance the transient stability but also ensure the steady-state stability.

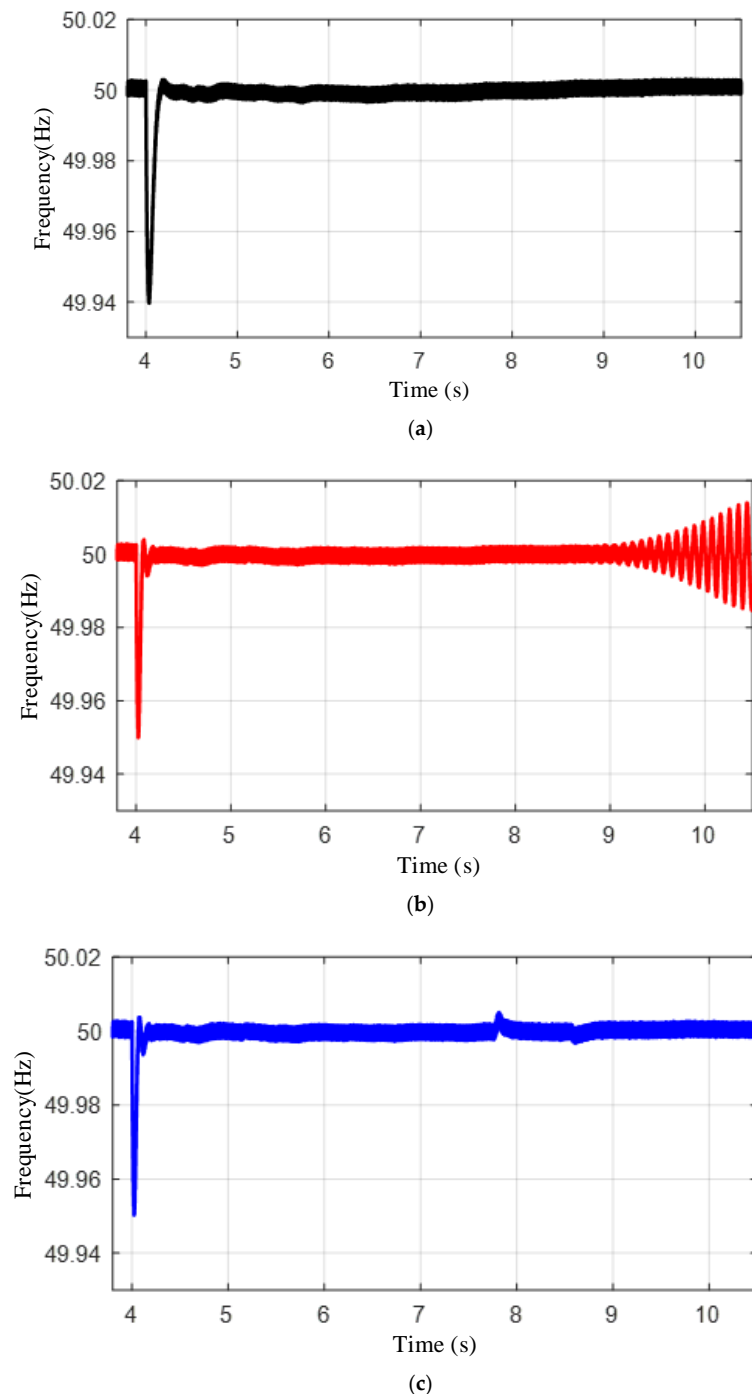


Figure 18. The AC system frequency disturbance in case 1 simulation between 3.8 s and 20 s. (a) The frequency disturbance without control. (b) The frequency disturbance with traditional control. (c) The frequency disturbance with the proposed control.

5. Conclusions

According to the theory analysis and simulation results, it can be concluded that the proposed combined frequency control strategy including wind power synchronous control and battery energy system supplementary control can efficiently improve the AC system's stability. The simulations show that the frequency drop with the proposed method can be decreased by 0.02 Hz. Specifically, the wide-area SOC of the considered battery energy storage system's supplementary control can ensure the energy of the high-SOC battery can be fully used, and the oscillations can be suppressed when the wide-area SOC is considered, which can help the multiconverter infeed system operation.

On the other hand, more fundamental battery characteristics could be considered in the future, such as the mechanism of aging, unbalance control and so on. We will examine these topics in our future work.

Author Contributions: Conceptualization, X.W. and X.Y.; methodology, X.W. and X.Y.; software, X.W. and X.Y.; validation, W.W., Y.W. and T.Z.; formal analysis, W.W., Y.W. and T.Z.; investigation, W.W., Y.W. and T.Z.; resources, C.L.; data curation, C.L.; writing—original draft preparation, Y.C.; writing—review and editing, Y.C.; visualization, X.W. and X.Y.; supervision, X.W. and X.Y.; project administration, X.W. and X.Y.; funding acquisition, X.W. and X.Y. All authors have read and agreed to the published version of the manuscript.

Funding: This research was funded by the Research Projects of Sichuan New Electric Power System Research Institute, grant number B7199723R005.

Data Availability Statement: Not applicable.

Conflicts of Interest: The authors declare no conflict of interest.

References

1. Li, B.; Chen, S.; Liu, T. Improved practical method for low-inertia VSC-HVDC stability analysis in weak system. *IET Gener. Transm. Distrib.* **2020**, *14*, 5072–5079. [\[CrossRef\]](#)
2. Jiang, Q.; Li, B.; Liu, T. Tech-Economic Assessment of Power Transmission Options for Large-Scale Offshore Wind Farms in China. *Processes* **2022**, *10*, 979. [\[CrossRef\]](#)
3. Li, B.; Cheng, T.; Jiang, Q.; Su, X.; Zhang, J.; Zhang, H. Faulty Feeders Identification for Single-phase-to-ground Fault Based on Multi-features and Machine Learning. *IEEE Trans. Ind. Appl.* **2023**, 1–11. [\[CrossRef\]](#)
4. Jiang, Q.; Zeng, X.; Li, B.; Wang, S.; Liu, T.; Chen, Z.; Wang, T.; Zhang, M. Time-Sharing Frequency Coordinated Control Strategy for PMSG-Based Wind Turbine. *IEEE J. Emerg. Sel. Top. Circuits Syst.* **2022**, *12*, 268–278. [\[CrossRef\]](#)
5. Jiang, Q.; Tao, Y.; Li, B.; Liu, T.; Chen, Z.; Blaabjerg, F.; Wang, P. Joint Limiting Control Strategy Based on Virtual Impedance Shaping for Suppressing DC Fault Current and Arm Current in MMC-HVDC System. *J. Mod. Power Syst. Clean Energy* **2023**, *101*, 1–11. [\[CrossRef\]](#)
6. Ghosh, S.; Isbeih, Y.J.; Bhattarai, R.; El Moursi, M.S.; El-Saadany, E.F.; Kamalasadnan, S. A Dynamic Coordination Control Architecture for Reactive Power Capability Enhancement of the DFIG-Based Wind Power Generation. *IEEE Trans. Power Syst.* **2020**, *35*, 3051–3064. [\[CrossRef\]](#)
7. Rather, Z.H.; Chen, Z.; Thogersen, P.; Lund, P. Dynamic Reactive Power Compensation of Large-Scale Wind Integrated Power System. *IEEE Trans. Power Syst.* **2014**, *30*, 2516–2526. [\[CrossRef\]](#)
8. Ouyang, J.; Tang, T.; Yao, J.; Li, M. Active Voltage Control for DFIG-Based Wind Farm Integrated Power System by Coordinating Active and Reactive Powers Under Wind Speed Variations. *IEEE Trans. Energy Convers.* **2019**, *34*, 1504–1511. [\[CrossRef\]](#)
9. Zhang, Y.; Ooi, B.T. Stand-Alone Doubly-Fed Induction Generators (DFIGs) With Autonomous Frequency Control. *IEEE Trans. Power Deliv.* **2013**, *28*, 752–760. [\[CrossRef\]](#)
10. Wang-Hansen, M.; Josefsson, R.; Mehmedovic, H. Frequency Controlling Wind Power Modeling of Control Strategies. *IEEE Trans. Sustain. Energy* **2013**, *4*, 954–959. [\[CrossRef\]](#)
11. Rodriguez-Amenedo, J.; Arnalte, S.; Burgos, J. Automatic generation control of a wind farm with variable speed wind turbines. *IEEE Trans. Energy Convers.* **2002**, *17*, 279–284. [\[CrossRef\]](#)
12. Zhang, X.; Zha, X.; Yue, S.; Chen, Y. A Frequency Regulation Strategy for Wind Power Based on Limited Over-Speed De-Loading Curve Partitioning. *IEEE Access* **2018**, *6*, 22938–22951. [\[CrossRef\]](#)
13. Rebello, E.; Watson, D.; Rodgers, M. Performance Analysis of a 10 MW Wind Farm in Providing Secondary Frequency Regulation: Experimental Aspects. *IEEE Trans. Power Syst.* **2019**, *34*, 3090–3097. [\[CrossRef\]](#)
14. An, G.; Jiang, Z.; Cao, X.; Liang, Y.; Zhao, Y.; Li, Z.; Dong, W.; Sun, H. Short-Term Wind Power Prediction Based on Particle Swarm Optimization-Extreme Learning Machine Model Combined with Adaboost Algorithm. *IEEE Access* **2021**, *9*, 94040–94052. [\[CrossRef\]](#)

15. Sun, Y.; Li, Z.; Yu, X.; Li, B.; Yang, M. Research on Ultra-Short-Term Wind Power Prediction Considering Source Relevance. *IEEE Access* **2020**, *8*, 147703–147710. [[CrossRef](#)]
16. Asghar, R.; Fulginei, F.R.; Wadood, H.; Saeed, S. A Review of Load Frequency Control Schemes Deployed for Wind-Integrated Power Systems. *Sustainability* **2023**, *15*, 8380. [[CrossRef](#)]
17. Lei, M.; Meng, K.; Jia, Y.; Li, C.; Jiang, H. Optimal configuration of flywheel energy storage based on wind storage system and cross particle swarm optimization. *Energy Energy Sav.* **2022**, *9*, 1–6+83.
18. Xu, Q.; Teng, W.; Wu, X.; Liu, Y.; Liang, S. Capacity configuration method of flywheel energy storage system for smoothing wind power fluctuation. *Energy Storage Sci. Technol.* **2022**, *11*, 3906–3914.
19. Ullah, K.; Basit, A.; Ullah, Z.; Albogamy, F.R.; Hafeez, G. Automatic Generation Control in Modern Power Systems with Wind Power and Electric Vehicles. *Energies* **2022**, *15*, 1771. [[CrossRef](#)]
20. Teleke, S.; Baran, M.E.; Bhattacharya, S.; Huang, A.Q. Optimal Control of Battery Energy Storage for Wind Farm Dispatching. *IEEE Trans. Energy Convers.* **2010**, *25*, 787–794. [[CrossRef](#)]
21. Jia, X.; Zhang, C.; Wang, L.Y.; Zhang, L.; Zhou, X. Early Diagnosis of Accelerated Aging for Lithium-Ion Batteries with an Integrated Framework of Aging Mechanisms and Data-Driven Methods. *IEEE Trans. Transp. Electrification* **2022**, *8*, 4722–4742. [[CrossRef](#)]
22. Li, S.; Zhao, P.; Gu, C.; Li, J.; Huo, D.; Cheng, S. Aging Mitigation for Battery Energy Storage System in Electric Vehicles. *IEEE Trans. Smart Grid* **2022**, *14*, 2152–2163. [[CrossRef](#)]

Disclaimer/Publisher’s Note: The statements, opinions and data contained in all publications are solely those of the individual author(s) and contributor(s) and not of MDPI and/or the editor(s). MDPI and/or the editor(s) disclaim responsibility for any injury to people or property resulting from any ideas, methods, instructions or products referred to in the content.